Oligodendrocyte-derived IL-33 functions as a microglial survival factor during neuroinvasive flavivirus infection

Geoffrey T. Norris[1], Joshua M. Ames[1], Steven F. Ziegler[1,2], Andrew Oberst[1,3,*]

[1]Department of Immunology, University of Washington, Seattle WA 98109, USA

[2]Immunology Program, Benaroya Research Institute, Seattle WA 98101, USA

[3]Lead Contact

[*]Correspondence: Oberst@UW.edu

Abstract

In order to recover from infection, organisms must balance robust immune responses to pathogens with the tolerance of immune-mediated pathology. This balance is particularly critical within the central nervous system, whose complex architecture, essential function, and limited capacity for self-renewal render it susceptible to both pathogen- and immune-mediated pathology. Here, we identify the alarmin IL-33 and its receptor ST2 as critical for host survival to neuroinvasive flavivirus infection. We identify oligodendrocytes as the critical source of IL-33, and microglia as the key cellular responders. Notably, we find that the IL-33/ST2 axis does not impact viral control or adaptive immune responses; rather, it is required to promote the activation and survival of microglia. In the absence of intact IL-33/ST2 signaling in the brain, neuroinvasive flavivirus infection triggered aberrant recruitment of monocyte-derived peripheral immune cells, increased neuronal stress, and neuronal cell death, effects that compromised organismal survival. These findings identify IL-33 as a critical mediator of CNS tolerance to pathogen-initiated immunity and inflammation.

KEYWORDS: West Nile virus, Zika virus, inflammation, neuroinflammation, microglia, disease tolerance,

Author Summary

The central nervous system (CNS) is an extraordinarily complex organ system with limited capacity for repair and renewal. When infectious pathogens invade the CNS, resulting immune responses must clear the pathogen while limiting immune-mediated

tissue pathology. IL-33 is an “alarmin” cytokine, whose release from dying cells can promote a variety of immune responses. IL-33 is expressed at high levels in the brain, and previous work has implicated signaling by IL-33 in CNS development as well as in the response to parasitic infection of the CNS. Here, we identify IL-33 as a key mediator of disease tolerance in the context of neuroinvasive infection with the flaviviruses West Nile virus and Zika virus. Notably, we find that IL-33 signaling is not involved in the clearance of virus from the brain; rather, IL-33 is required to promote the survival and reprogramming brain-resident immune cells (microglia). When IL-33 signaling is disrupted in mice, flavivirus infection results in defective microglial activation, increased death of both microglia and neurons, increased invasion of the brain by peripheral immune cells, and increased host death. This work suggests that IL-33 is a key mediator of host tolerance upon neuroinvasive flavivirus infection.

Introduction

Immune responses within the central nervous system (CNS) must both clear pathogens and avoid immune-mediated damage to the complex neuronal architecture that makes up this organ system. As the resident cells immune cells of the CNS, microglia are ideally positioned to mediate both pathogen elimination and tissue preservation. Microglia are long-lived tissue resident macrophages unique in their origin entirely from embryonic yolk sac progenitors with no contribution from other hematopoietic compartments, barring significant CNS disease[1]. Recent advances have described multiple roles for microglia in both CNS homeostasis and upon its perturbation [2,3]. Recent studies have also revealed

71 mechanisms of microglial function during CNS viral infection [4], where microglia have been
72 shown to contain infection and tissue damage during acute infection, while mediating
73 neuronal and tissue damage if aberrantly activated during recovery. These findings
74 highlight the pleotropic nature of microglial functions in the CNS, and point to a need to
75 better understand the signals that promote the distinct roles of this cell type.

76 The cytokine IL-33 is a member of the IL-1 family of alarmin cytokines. IL-33 is
77 normally released by damaged or necrotic cells, signaling in a paracrine manner to
78 bystanders expressing the IL-33 receptor ST2 (encoded by *Il1rl1).* IL-33/ST2 signaling
79 has divergent roles in peripheral immune responses, notably contributing to both immune
80 cell activation and tissue homeostasis, including roles in promoting macrophage survival
81 [5]. Notably, IL-33 is highly expressed the CNS, and several roles for IL-33 in CNS
82 development and pathology have been identified, including promotion of synaptic pruning
83 and extracellular matrix remodeling by microglia [6,7], and promotion of recovery from spinal
84 cord injury through macrophage signaling [8]. IL-33 signaling from astrocytes to microglia
85 has also been identified as a driver of protective immune responses to *Toxoplasma gondii*
86 in the brain [9]. However, while the related alarmin IL-1 has been implicated in promoting
87 sequalae to flavivirus infection [10], whether IL-33 contributes to beneficial or pathogenic
88 responses to neurotropic viral infection remains unexplored.

89 Since its arrival in the Western Hemisphere, the flavivirus West Nile virus (WNV)
90 has become a significant threat to public health, with the majority of disease burden
91 resulting from neuroinvasive infection [11–13]. Recent studies using an attenuated strain of
92 West Nile virus, termed WNV-E218A, as well as a less neurovirulent form of the related
93 Zika virus (ZIKV-Dakar), have shown bivalent roles for resident microglia in promoting

94 neurological pathology and cognitive sequelae to flavivirus infection, while also
95 contributing to host survival during acute infection. [10,14–16]. Specifically, during acute
96 infection microglia were shown to phagocytose neuronal processes the murine
97 hippocampus, a phenomenon that limits viral dissemination while causing disease
98 sequelae specific to episodic spatial memory [17]. However, pharmacological removal of
99 microglia yielded decreased host and neuronal survival, with minimal changes in viral titer
100 [16], suggesting that microglia play essential roles in host survival during neuroinvasive viral
101 infection.

102 In this study, we show that IL-33 signaling promotes survival during flavivirus
103 infection, an effect apparently independent of a role for IL-33 in viral control. We found
104 that following CNS infection oligodendrocyte numbers acutely decrease, with IL-33
105 expression by oligodendrocytes necessary for host survival, implicating release of IL-33
106 from dying oligodendrocytes. The target of IL-33 signaling was primarily microglia, as
107 mice with specific deletion of ST2 on microglia succumbed more readily to CNS disease.
108 In these mice, we found defects in microglial activation and survival, leading to enhanced
109 BBB breakdown, increased monocyte extravasation and neuronal apoptosis. Together,
110 our studies reveal a source for CNS IL-33 during flavivirus infection and highlight its role
111 in promoting microglial fitness in this setting. These findings suggest that IL-33 signaling
112 is required for CNS tolerance to the inflammatory response triggered by neuroinvasive
113 flavivirus infection.

114

115 **Results**

116 **IL-33/ST2 signaling promotes survival upon neuroinvasive flavivirus infection**

117 We sought to assess the role of IL-33 and its receptor ST2 in controlling the CNS
118 pathogenesis of flavivirus infection. In order to isolate roles for IL-33 and ST2 within the
119 CNS, we used an established model of intracranial infection with an attenuated form of
120 WNV (WNV-E218A), a model in which most wild-type mice survive infection but display
121 CNS pathology and sequelae [14,18] **(Fig S1A)**. To study the role of the IL-33/ST2 pathway
122 in these infection models, we infected *Il1rl1*$^{-/-}$, *Il33*$^{-/-}$, and wild type congenic animals with
123 WNV-E218, then monitored their survival. While ~75% of wild type animals survived
124 infection, both *Il1rl1*$^{-/-}$ and *Il33*$^{-/-}$ mice were significantly more susceptible to WNV-E218A
125 infection, displaying reduced survival and enhanced weight loss **(Figs 1A and S1B)**. We
126 reasoned that this increase in susceptibility could be due to a failure to control viral
127 replication within the CNS. To test this, we titered virus from the cortex, hippocampus,
128 cerebellum, brainstem, and peripheral organs of *Il1rl1*$^{-/-}$, *Il33*$^{-/-}$, and B6/J infected mice
129 at 7 days post-infection (DPI), a timepoint that corresponds to peak disease [14]. While no
130 virus was detected in the periphery of these animals, only the cortex exhibited varying
131 degrees of infectious virus titer **(Fig 1B)**. Surprisingly, *Il33*$^{-/-}$ animals displayed lower
132 levels of viral titers compared to controls while *Il1rl1*$^{-/-}$ titers were higher than WT. No
133 differences in viral titer were seen in other CNS regions.
134 Since WNV-E218A is an attenuated flavivirus sensitive to the interferon stimulated
135 gene IFIT1 [19], we tested the effects of IL-33 and ST2 deletion with a wild-type isolate of
136 the related flavivirus Zika virus, termed ZIKV-Dakar. While intracranial infection of
137 congenic WT animals yielded ~90% survival, *Il1rl1*$^{-/-}$ mice were significantly more
138 susceptible to infection with survivorship at ~70%. *Il33*$^{-/-}$ mice had a further decrease in
139 survivorship at ~30% with both genotypes showing increased weight loss **(Figs 1C and**

140 **S1C)**. Upon examination of viral titers from the tissues of these animals we observed that,
141 similarly to WNV-E218A infection, no virus was detected in peripheral tissues **(Fig. 1D)**.
142 Within the CNS only the brainstem showed differences in viral titer upon loss of IL-33/ST2
143 signaling upon ZIKV-Dakar infection, with *Il1rl1*$^{-/-}$ mice showing lower levels of infectious
144 virus than either WT or *Il33*$^{-/-}$ animals **(Fig. 1D)**. We also assessed the role of IL-33/ST2
145 signaling in models of peripheral flavivirus infection, and observed increased mortality
146 and weight loss in *Il1rl1*$^{-/-}$ mice (**Figs S1D and S1E**). Further, titering infected tissues of
147 these mice showed no statistically significant differences in CNS or peripheral organ viral
148 titer **(Fig S1F).** Collectively these results suggest that the IL-33/ST2 signaling pathway is
149 important for host survival upon neuroinvasive WNV infection, but that this activity is
150 independent of a role in controlling viral replication or dissemination.
151
152 **Oligodendrocyte-derived IL-33 promotes survival upon neuroinvasive WNV**
153 **infection**
154 Since our studies of knockout mice suggested a role for IL-33 in promoting survival
155 to neuroinvasive flavivirus infection, we next sought to assess the source of IL-33 in this
156 setting. We first analyzed the expression and localization of IL-33 in the uninfected CNS
157 and found that IL-33 was exclusively expressed in either oligodendrocytes (Olig2+) or
158 astrocytes (GFAP+) in concordance with prior studies [8,9] **(Fig 2A).** Since IL-33 signaling
159 is associated with its release from dying cells, the loss of IL-33^{+} cells has been used as a
160 surrogate for IL-33 activity [8,9]. To examine the release of IL-33 by Olig2 or GFAP-
161 expressing cells, we intracranially infected C57Bl6/J mice with WNV-E218A and
162 sacrificed animals during peak CNS disease at 7 DPI, preserving their brains for IHC

163 analysis. Examining hippocampal sub regions of CA3, an area known for synaptic
164 stripping and inflammation during CNS infection, we observed a loss of both IL-33+
165 astrocytes and IL-33+ oligodendrocytes 7 days post-infection (**Figs 2B and 2C**).

166 Since IL-33 release is classically associated with cell death we next quantified the
167 number of both astrocytes and oligodendrocytes post-infection. While total GFAP+
168 astrocyte numbers were stable (**Fig S2A**), Olig2+ oligodendrocyte cell numbers were
169 decreased not only in CA3 sub regions but across the CNS post-infection **(Figs 2D and**
170 **2E)**. Given the loss of Olig2+IL-33+ cells in regions of known synaptic stripping and the
171 observation that oligodendrocyte numbers decrease across the CNS during infection, as
172 well as previous studies that have shown oligodendrocyte cell death upon flavivirus
173 infection *in vitro* and *in vivo*[20–22], we hypothesized that oligodendrocytes represented a
174 probable source of released IL-33 following neuroinvasive WNV infection. To test this, we
175 crossed *Plp1*$^{ERT2Cre/+}$ mice with *Il33*$^{fl/fl}$ animals to generate mice lacking IL-33 in
176 oligodendrocytes. We first confirmed that tamoxifen treatment induced the excision of IL-
177 33 from Olig2+ cells without impacting total Olig2+ cell number **(Figs S2B-S2C)**. We next
178 intracranially infected tamoxifen-treated *Plp1*$^{ERT2Cre/+}$::*Il33*$^{fl/fl}$ mice, as well as Cre-negative
179 littermates, with WNV-E218A. Strikingly, Cre+ animals exhibited a survival phenotype
180 closely matching that of global IL-33 deficient animals **(Fig 2F)**. Collectively, these data
181 indicate that oligodendrocyte loss is widespread following CNS WNV infection, and that
182 oligodendrocyte-derived IL-33 promotes host survival.

183

184 **The IL-33/ST2 signaling axis promotes survival independent of adaptive immunity**
185 **during neuroinvasive flavivirus infection**

186 The IL-33/ST2 signaling pathway has well-defined roles in T cell activation during
187 viral infection, with CD8+ [23], CD4+ [24], and Treg cells [25] implicated. Notably, these three
188 adaptive immune cell types are all critical for WNV host defense [26,27]. We therefore
189 wondered if the survival defect observed in *Il33*$^{-/-}$ or *Il1rl1*$^{-/-}$ mice upon neuroinvasive
190 flavivirus infection was due to altered T cell recruitment or activation. To examine this, we
191 infected both WT and *Il33*$^{-/-}$ mice intracranially with WNV-E218A or ZIKV-Dakar and
192 sacrificed each at 7 days post-infection, removing and processing the brain parenchyma
193 for examination of T cell responses by flow cytometry. Remarkably, there was no change
194 in the number of adaptive effector cells in response to WNV-E218A in *Il33*$^{-/-}$ animals **(Fig**
195 **3A)**. While there was a modest increase in overall T cell number with ZIKV-Dakar
196 infection in *Il33*$^{-/-}$ mice, no differences in Tconv, Treg, or CD8 T cells were seen in *Il33*$^{-/-}$
197 animals with ZIKV-Dakar infection, with MFIs of CD44 and CD69 unchanged in Tconv
198 and CD8 T cells **(Fig 3B)**. Despite these data, and given the essential role of CD8 T cells
199 in CNS protection during WT WNV infection [28], we sought to functionally test their role by
200 depleting CD8 T cells from WT animals and infecting both control and CD8 T cell-depleted
201 mice with WNV-E218A to monitor survival **(Fig S3A)**. Despite robust CD8 T cell depletion,
202 especially among NS4b+ CD8 T cells specific to WNV **(Fig S3B),** no change in survival
203 or weight loss was observed (**Figs S3C and S3D**).
204 To further assess a role for IL-33/ST2 signaling in adaptive immunity, we sought
205 to define which leukocyte subsets express ST2 during infection. To do this, we analyzed
206 both mock and WNV-E218A infected WT mice by flow cytometry at 7 DPI to investigate
207 ST2 expression on CNS immune cells (**Fig S3E**)**.** While HBSS-injected animals showed
208 highest ST2 expression on CD8+ and CD4+ T cells (**Fig 3C**), during infection we observed

209 the highest proportion of ST2+ cells among Tregs (~8%), followed by Tconv (~2%), and
210 CD45+Non-LymphoidCD11b- cells (~1%); the latter likely representing meningeal innate
211 lymphoid type 2 cells (ILC2s) which are known to express ST2 [29] and exhibited the highest
212 levels of ST2 by MFI **(Figs 3D and S3F)**. As Tregs are known to be critical for host survival
213 following WNV infection and exhibited the highest proportion of ST2 positivity by any of
214 the examined leukocytes **(Figs 3D and S3F)** we tested whether lack of IL-33/ST2
215 signaling on Treg cells contributed to the observed survival defects following
216 neuroinvasive flavivirus infection. To assess this, we crossed *Foxp3*$^{ERT2Cre+/y}$ mice with
217 *Il1rl1*$^{fl/fl}$ animals, to delete ST2 on FOXP3-expressing Treg cells. After confirming that ST2
218 expression was deleted on both splenic and tissue Tregs prior to infection **(Fig S3G)** we
219 intracranially infected mice with both intact (*Foxp3*$^{Ert2Cre+/y}$:: *Il1rl1*$^{fl/+}$) and deleted
220 (*Foxp3*$^{Ert2Cre+/y}$:: *Il1rl1*$^{fl/fl}$) Treg ST2 with ZIKV-Dakar. Despite effective ST2 deletion on
221 Tregs we observed no difference in survival **(Fig 3E)** or weight loss **(Fig S3H)** between
222 groups, indicating that Treg expression of ST2 is dispensable for CNS flavivirus defense.
223 As an alternative approach to assess a role for Tregs in survival following neuroinvasive
224 WNV infection, we boosted the number and reactivity of Tregs via administration of IL-2
225 complexes [30] following CNS infection of WNV-E218A. While both the number of Tregs
226 and expression of effector proteins CD25 and GITR were increased in circulation 9 DPI
227 **(Figs S3I and S3J),** no effect of survival or weight loss to WNV-E218A infection was
228 observed in response to IL-2 complex administration **(Fig S3K and S3L)**. Collectively,
229 these data suggest that while ST2 expression is prominent on adaptive immune cells
230 during peak CNS disease, signaling via the IL-33/ST2 axis on adaptive immune cells is
231 dispensable for direct CNS immune responses to flaviviruses.

232

233 **IL-33 signaling is required for normal microglial activation following neuroinvasive**
234 **WNV infection**

235 We next sought to identify an effector cell population for the IL-33/ST2 axis during
236 CNS flavivirus infection. Given our negative findings regarding roles for lymphocytes in
237 this process, as well as recent work highlighting a role for IL-33 signaling in microglial
238 activation [6,7,31], we tested whether IL-33 release is associated with microglial activation in
239 the CA3 region. To do this, we infected wild-type mice with increasing doses of WNV-
240 E218A, then assessed both the number of IL-33-positive cells and microglial activation
241 by staining for the macrophage somatic marker Iba1 and the phagosomal marker CD68.
242 We observed that IL-33 staining decreased in both the pyramidal layer and stratum lucidi
243 of the CA3 region with increasing infectious doses of WNV-E218A **(Figs 4A and 4B)**,
244 consistent with IL-33 release in these regions. Furthermore, loss of IL-33 in both regions
245 correlated with increased Iba1 while CD68 staining was also increased in both regions
246 **(Figs 4A and 4B).**

247 These data suggested that IL-33/ST2 signaling may drive microglia activation
248 following WNV infection. To test this more directly, we analyzed microglial activation by
249 quantifying the MFI of the macrophage marker Iba1 by IHC in both WT and *Il1rl1*$^{-/-}$ mice
250 7 DPI with WNV-E218A. We observed a striking impairment of microglial activation 7 days
251 post-infection in CA3, deep cerebellar nuclei (DCN), and cortex of *Il1rl1*$^{-/-}$ mice **(Figs 4C**
252 **and 4D)**. Importantly, mock-infected B6/J and *Il1rl1*$^{-/-}$ mice did not differ in Iba1 MFI,
253 indicating no baseline effect of IL-33 on Iba1 intensity **(Figs S4A and S4B).** Further, when
254 we analyzed B6/J and *Il1rl1*$^{-/-}$ mice at 10 DPI, this activation phenotype was maintained,

255 suggesting IL-33 signaling may contribute to persistent microglial activation phenotypes
256 post-infection **(Figs S4C and S4D)**. Despite its reported role in synaptic stripping by
257 activated microglia in diverse CNS pathologies [32], complement deposition of C1q protein
258 at 7DPI was not affected by the absence of IL-33 during infection **(Figs S4E and S4F).**

259 To directly test whether the loss of IL-33/ST2 signaling on microglia, and resulting
260 impairment in activation, was responsible for the increased susceptibility to WNV infection
261 we previously observed in IL-33- and ST2-deficient mice, we crossed *Cx3cr1*^{Ert2Cre} mice
262 with *Il1rl1*$^{fl/fl}$ animals. In resulting *Cx3cr1*$^{Ert2Cre/+}$*:: Il1rl1*$^{fl/fl}$ animals, tamoxifen administration
263 causes ST2 excision in all tissue resident macrophages. However, we used a previously-
264 defined strategy of administering tamoxifen, then resting mice for one month to allow
265 turnover of peripheral, but not brain-resident, macrophage populations **(Goldmann et al.,**
266 **2013)**. We first confirmed microglial ST2 excision in naïve mice one-month post
267 tamoxifen treatment by MAC sorting whole brain homogenate with CD11b beads and
268 subsequent RT-PCR. After first confirming purity of our samples by flow cytometry **(Figs**
269 **S4G-S4H),** we observed downregulation of the ST2 receptor only in *Cx3cr1*$^{Ert2Cre/+}$*::*
270 *Il1rl1*$^{fl/fl}$ sorted microglia by RT-PCR **(Fig S4I).** Next, we infected tamoxifen-treated
271 *Cx3cr1*$^{Ert2Cre/+}$*:: Il1rl1*$^{fl/fl}$ and *Cx3cr1*$^{+/+}$*:: Il1rl1*$^{fl/fl}$ animals intracranially with WNV-E218A and
272 monitored their survival. While animals with intact ST2 signaling on brain macrophages
273 survived at rates comparable to WT animals, *Cx3cr1*$^{ERT2Cre/+}$*:: Il1rl1*$^{fl/fl}$ mice displayed
274 significantly increased mortality **(Fig 4E)** and weight loss (**Fig S4J**), comparable to that
275 observed when this infection model was applied to mice globally lacking ST2 or IL-33
276 **(Fig. 1A).** A recent study identified ST2 expression on peripheral sensory neurons in the
277 context of sterile skin injury [35]. To test whether neuronal ST2 expression contributed to

278 our phenotypes we crossed *Camk2a*$^{Cre/+}$ mice with *Il1rl1*$^{fl/fl}$ mice generating mice with
279 intact (*Camk2a*$^{+/+}$*:: Il1rl1*$^{fl/fl}$) and deficient *(Camk2a*$^{Cre/+}$*: Il1rl1*$^{fl/fl}$*)* neuronal ST2 signaling.
280 Upon WNV-E218A infection no change in survival (**Fig S4K**) or weight loss (**Fig S4L**) was
281 seen. Together, these findings support the idea that ST2 expression on microglia is
282 responsible for both macrophage activation and host survival in response to WNV
283 infection.
284
285
286 **Brain macrophages from *Il33*$^{-/-}$ mice exhibit enhanced inflammatory and stress**
287 **responses post-infection**
288 In light of these phenotypes and to identify the transcriptional programs initiated by
289 IL-33 on brain macrophages following infection, we isolated hippocampal brain
290 macrophages (a population expected to include both microglia and recruited peripheral
291 monocyte-derived macrophages) using F4/80 mediated MACS from WT and *Il33*$^{-/-}$ mice
292 7 days after intracranial WNV-E218A infection and processed them for RNA sequencing.
293 **(Fig 5A)**. Before sequencing, MAC-sorted sample purity was determined by flow
294 cytometry**(Figs S5A-S5C).** Following RNAseq analysis, we first performed principal
295 component analysis and observed clustering of samples by both genotype and infection
296 status **(Fig 5B)**. Analysis of RNAseq datasets revealed 251 significantly differentially
297 expressed genes when comparing B6/J and IL-33 deficient macrophages during infection
298 **(Fig 5C)**. Additionally, and consistent with previous reports, we observed a number of
299 differentially expressed genes in vehicle-treated IL-33-deficient animals relative to wild-
300 type controls, consistent with homeostatic roles for IL-33 [31] **(Fig S5D)**. We next performed

301 Gene Set Enrichment Analysis (GSEA) using Hallmark gene sets that may be
302 differentially expressed during infection. While the top gene sets enriched in IL-33-
303 deficient cells relative to wild-type **(Fig 5D and S5E)** during infection included predictable
304 dysregulation of inflammatory processes **(Figs S5D and S5F)**, we were surprised to
305 observe a number of cell metabolism and stress gene sets enriched including: Fatty Acid
306 Metabolism **(Fig S5G)**, Oxidative Phosphorylation **(Fig S5H)**, Hypoxia **(Fig S5I)** and
307 Apoptosis **(Fig S5J).** Collectively, these data point to a dysregulation of brain macrophage
308 activation following WNV-E218A infection in *Il33*$^{-/-}$ mice typified by altered metabolic state
309 and upregulation of cell stress pathways, including apoptosis.
310
311 **IL-33 functions as a microglial survival factor limiting CNS pathology following**
312 **WNV infection**
313 Previous studies have shown a role for IL-33 in the metabolic support of
314 macrophage survival [5,31] . Since we observed a lack of macrophage activation and
315 hypertrophy in ST2-deficient mice, as well as upregulated cell stress pathways in brain
316 macrophages isolated from *Il33*$^{-/-}$ mice, we hypothesized that brain macrophage viability
317 may be impacted subsequent to intracranial WNV-E218A delivery in the absence of IL-
318 33/ST2 signaling. To quantify this, we examined brain macrophage (CD11b+F4/80+)
319 viability in *Il1rl1*$^{-/-}$ mice post-infection by flow cytometry. Looking 7 days post-infection
320 with WNV-E218A we observed that in whole brain samples, macrophages, but not other
321 infiltrating leukocyte populations exhibited higher proportions of cell death as quantified
322 by the viability dye ZombieNIR **(Fig 6A).** To confirm this phenotype, we next performed
323 IHC on B6/J and *Il33*$^{-/-}$ mice infected with WNV-E218A at 7 days post infection, using the

macrophage marker Iba1 and terminal apoptotic marker cleaved-caspase 3 (CC3). We observed marked macrophage apoptosis in the CA3 of *Il33*$^{-/-}$ mice with WNV-E218A infection **(Figs 6B and 6C)** and also in hippocampal CA1 7 DPI with ZIKV-Dakar (**Figs S6A and S6B).**

A key driver of pathology in neuroinvasive WNV disease is the entry of peripheral monocytes to the CNS [36–38]. Given the blunted activation and enhanced apoptosis observed in resident microglia in the absence of IL-33/ST2 signaling, we wondered if peripheral monocytes would be recruited in greater numbers in these animals to compensate for—or in response to—dysregulated microglial responses. To assess this, we examined the number of brain-engrafted monocytes in B6/J and *Il1rl1*$^{-/-}$ by flow cytometry following intracranial WNV-E218A infection and observed a marked increase in the number of monocytes in whole brain homogenates **(Fig 6D)**. Enhanced monocyte engraftment post-infection was also corroborated by quantifying CD68+Iba1- cells in CA3 and cerebellum of B6/J and *Il33*$^{-/-}$ mice at 7DPI by immunohistochemistry of infected brain tissue (**Figs 6E and 6F**)

Given the strong phenotypes seen with both global and microglial deletion of IL-33 signaling on host and brain macrophage survival, we next sought to examine CNS pathologic processes that may underlie host demise. To examine neuronal pathology we stained hippocampal region CA3 and cerebellum in both B6/J and *Il33*$^{-/-}$ mice infected with WNV-E218A using antibodies against the neuronal distress marker phospho-c-Jun [39] and endogenous mouse IgG to mark blood-brain barrier (BBB) leakage. Strikingly, we saw an increase in CA3 IgG deposition and phospho-c-Jun+ cells in both areas of *Il1rl1*$^{-/-}$ animals **(Figs 6G and 6H)**. We also observed increased staining for the astrocyte

347 activation marker GFAP in these regions, as well as increased phospho-c-Jun expression
348 in mossy fibers of CA3 of *Il1rl1*$^{-/-}$ animals, an early phenotype of neurodegeneration
349 observed in many models of CNS pathology [40] (**Figs 6I and 6J**). Collectively these data
350 are consistent with a state of increased monocyte ingress and vascular leak, neuronal
351 distress, and astrocyte hyperactivity in *Il33*$^{-/-}$ mice following flavivirus infection.

352 Lastly, we examined apoptotic neurons in hippocampal CA3 and cerebellum by
353 quantifying cleaved-caspase 3 positive NeuN expressing cells and found increased
354 neuronal apoptosis in *Il33*$^{-/-}$ mice at 7 DPI in both regions **(Figs 6K and 6L)**. Together,
355 these data suggest that IL-33/ST2 signaling is required during intracranial flavivirus
356 infection to promote microglial viability. Our findings indicate that in the absence of IL-33
357 signaling, flavivirus infection leads to microglial apoptosis, ingress of pathogenic,
358 peripheral monocyte-derived cells to the CNS, neuronal distress, astrocyte hyperactivity,
359 and subsequent enhanced neuronal apoptosis and host demise.

360

361 **Discussion**

362 This study defines IL-33 as an oligodendrocyte-derived survival factor for microglia, and
363 suggests that IL-33 is required during viral infection to promote normal microglial
364 activation. In its absence, we observed wide-ranging defects in neuronal survival, blood-
365 brain barrier integrity, and peripheral monocyte infiltration, culminating in reduced host
366 survival. While the work detailed here does not define a mechanism for oligodendrocyte
367 release of IL-33, previous studies have demonstrated profound WNV-induced death of
368 oligodendrocytes *in vitro,* [20], from cultured explants [21]**,** and *in vivo* during peripheral
369 infection [22]**.** While these studies mainly indicated apoptotic death of oligodendrocytes,

370 other works have shown that oligodendrocytes express low levels of caspase 8 [41], a
371 mediator of death-receptor induced apoptosis, and that TNF is a robust inducer of
372 oligodendrocyte necrosis/necroptosis [42], implying that oligodendrocytes may be poised
373 for pro-inflammatory cell death, especially during viral infection. These data, in addition
374 to the finding that IL-33 reactivity is reduced, but not eliminated, by caspase 7 during
375 apoptosis [43] suggests that oligodendrocytes may undergo non-apoptotic cell death to
376 release IL-33 during neurotropic viral infection. Future studies will define the inducers
377 and mechanisms underlying these effects.

378 Our work also indicates that IL-33 signaling on adaptive immune populations does
379 little to affect survival at least in direct intracranial infection of flaviviruses. This is despite
380 our observation that ST2 expression was most widely seen on adaptive immune
381 populations at either resting state or during peak infection. This may be attributable to
382 reports that ST2 expression on various immune cells is very short-lived , as in the case
383 of splenic CD8 T cells in LCMV infection [23], or can shift in response to inflammatory
384 context such as its upregulation on macrophages and Natural Killer cells in models of
385 airway smoke exposure [44]. Despite observing limited ST2 expression on microglia, ST2
386 deletion on microglial cells did impact survival phenotypes in a manner similar to germline
387 knockout of ST2. Still, future studies may need to employ multiple timepoints, possibly on
388 an hourly timescale, to detect ST2 expression by protein on microglia.

389 While our studies observed enhanced expression of inflammatory and cell stress
390 gene sets on microglial populations in response to WNV infection, we were technically
391 limited in our sorting of F4/80+ cells, which at 7 DPI include both microglia and engrafted
392 monocyte-derived macrophages. Future experiments delineating resident microglia via

393 genetic fate-mapping and crossing to appropriate knockout strains may be required, as
394 no definitive microglial marker separating these cell types in disease states currently
395 exists.

396 Notably, the effect of IL-33 on host defense was not due to a failure of viral
397 clearance, as mice deficient in IL-33 signaling had equivalent viral titers at peak disease
398 timepoints and those that survived acute infection eventually cleared virus from CNS
399 tissues. Previous data have indicated a requirement for microglia in CNS WNV infection,
400 with deletion pharmacologically [16] or genetically [18] yielding decreased host survival.
401 However, the CNS of mice with pharmacologic microglial depletion also showed higher
402 levels of infectious virus and a blunted adaptive immune response, contrary to what was
403 observed here. This suggests that IL-33 signaling may drive a subset of microglial
404 functions related to survival and disease tolerance in the context of viral infection, and
405 that in its absence microglia may still participate in viral control. There may also be
406 differences between genetic and pharmacological depletion of microglia, as WNV-E218A
407 infection of microglia-deficient *Il34*$^{-/-}$ mice revealed decreased neuronal and host survival
408 with no change to CNS viral titer [18], similar to our data.

409 While the presence of microglia within the virally-infected CNS is clearly beneficial
410 for host and neuronal survival, how are microglia providing their neuroprotective effect
411 independent of effects on viral titer? The provision of secreted factors by microglia to
412 neurons directly or through supporting cells is one obvious possibility. Both TGF-β and
413 IGF-1 have been shown to be secreted by microglia during spinal cord injury and
414 observed to promote neuronal survival at the injury site [45]**.** The anti-inflammatory cytokine
415 IL-10, which is secreted by microglia in response to bacterial infection [46] may also be

416 responsible for tuning the CNS inflammatory milieu and ensuring neuroprotection.
417 Another possibility is microglial secretion of brain-derived neurotrophic factor (BDNF)
418 which is elicited by microglia during models of nerve injury and alters neuronal activity [47].
419 Microglial neuroprotection may also be mediated by synaptic stripping, preventing
420 aberrant neuronal activity at sites of infection from "spillover" to otherwise healthy
421 neuronal tissue.

422 IL-33 has recently emerged as a critical factor mediating macrophage survival in
423 multiple settings. For example, IL-33 signaling was shows to promote survival in red pulp
424 macrophage development [5] as well as altering microglial metabolic functioning [31]. Our
425 findings join other recent studies implicating IL-33 signaling on microglia as essential to
426 tune CNS function during development [6] and in adulthood [7]**.** In implicating IL-33 as a
427 promoter of microglia-mediated disease tolerance (rather than a driver of viral clearance
428 [48,49]) our findings highlight the pleotropic functions of microglia in both homeostasis and
429 disease. Our work also suggests that potentiating IL-33 signaling in the CNS could
430 ameliorate pathology and sequelae associated with neurotropic flavivirus infection.

431

432 **Materials and Methods**

433 **Mice**

434

435 B6/J (000664), *Il33*$^{fl/fl}$ (030619) *Cx3cr1*$^{ERT2Cre/\ ERT2Cre}$ (020940), *Plp1*$^{ERT2Cre/ERT2Cre}$
436 (005975), Aldh1l1$^{ERT2cre/\ ERT2cre}$ (029655), and *Camk2a*$^{Cre/Cre}$ (005359) mice were obtained
437 from Jackson Laboratories. C57BL/6J (B6/J) controls were either obtained commercially
438 (Jackson Laboratories) or, for control animals in experiments using transgenic mouse

439 strains, WT mice were bred in-house. *Il33*$^{-/-}$ (Originally from Dirk Smith at Amgen) and
440 Foxp3$^{ERT2Cre/y}$ (PMID: 18387831):: *Il1rl1*$^{fl/fl}$ mice were obtained from the Ziegler lab
441 (Benaroya Research Institute). *Il1rl1*$^{-/-}$ (ST2$^{-/-}$) (PMID: 10727469) mice were provided by
442 the Von Moltke lab (University of Washington). Mice in this study were bred and housed
443 under specific-pathogen free conditions at the University of Washington.
444
445 **Tamoxifen and in vivo injections**
446
447 To induce Cre activity in Cre-ERT2 mice, 100 uL of Tamoxifen (Sigma) at 20 mg/mL
448 dissolved in corn oil (Sigma) was injected every day for 5 consecutive days with mice
449 analyzed one month later. For CD8 T cell depletion mice were injected on days -1, 2, 5,
450 and 8 post-infection with 200 ug of αCD8 (Clone 2.43 BioXcell) or control IgG antibody in
451 200 uL PBS (PMID: 30143586). Depletion was confirmed by obtaining blood from the
452 retro orbital sinus 6DPI. To induce Treg expansion (PMID: 30291203) the JES6-1 αIL-2
453 antibody was mixed at a 2:1 molar ratio with IL-2 for 30 minutes at 37^0 C in PBS. Mice
454 were injected daily with a complex of 1 ug IL-2 (Peprotech) and 5 ug JES6-1 (BioXcell)
455 intraperitoneally on days 2-4 post-infection in a total volume of 200 uL. Expansion was
456 confirmed by obtaining blood from the retro orbital sinus at 9DPI.
457
458 **Viruses**
459
460 WNV-Tx was provided by Mike Gale of the University of Washington. WNV-E218A and
461 ZIKV-Dakar strains utilized for intracranial infections were obtained from Robyn Klein at

462 Washington University in St Louis. WNV-NS5-E218A contains a single point mutation in
463 the gene encoding 2′-*O*-methyltransferase (PMID: 31611100). Mice were deeply
464 anesthetized and intracranially administered 2e4 plaque-forming units (p.f.u.) of WNV-
465 NS5-E218A or 1e6 PFU of ZIKV-Dakar as described previously (PMID: 31235930).
466 Viruses were diluted in 20 µl of Hank's balanced salt solution (HBSS) and injected into
467 the third ventricle of the brain with a guided 29-guage needle. Mock-infected mice were
468 intracranially injected with 20 µl of HBSS. Footpad infections were performed by injection
469 of 100 PFU WNV in 50 µL of HBSS into a rear footpad as previously described (PMID:
470 28366204). BHK21 cells were used for quantification of WNV Titers while Vero cells were
471 used for titering ZIKV-Dakar as described (PMID: 24510289).
472
473 Infected mice were monitored daily for weight loss and presentation of clinical signs of
474 disease, including hunched posture, ruffled fur, hindlimb weakness, and paresis. Severity
475 of paresis was defined as follows: mild – partial loss of motor function in one hind limb;
476 moderate – com- plete or nearly complete loss of motor function in one hind limb or partial
477 loss of motor function in both hind limbs; severe – complete or nearly complete loss of
478 motor function in both hind limbs and/or pronounced ataxia. Mice reaching a moribund
479 state or losing more than 30% of initial body weight were euthanized as performed
480 previously (PMID:28366204). All experiments were performed in both male and female
481 2-4 month old mice, in accordance with protocols approved by the University of
482 Washington Animal Care and Use Committee (IACUC).
483
484 **Measurement of viral burden**

485

486 WNV- or ZIKV-infected mice were sacrificed and tissues were collected, weighed, and
487 homogenized with Precellys zirconia beads in a Precellys 24 homogenizer in 500 µl of
488 PBS, and stored at –80 °C until virus titration. Thawed samples were clarified by
489 centrifugation (2,000 × g at 4 °C for 10 min), and then diluted serially before infection of
490 BHK21 cells for WNV or Vero cells for ZIKV titers. Plaque assays were overlaid with low-
491 melting point agarose, fixed 4 days later with 4% formaldehyde, and stained with crystal
492 violet. Viral burden was expressed on a $\log_{10}$ scale as p.f.u. per gram of tissue.

493

494 **Tissue preparation and CNS leukocyte isolation**

495

496 All tissues harvested from mice for subsequent immunohistochemical, MACs, qRT-PCR,
497 protein, virologic, or flow cytometric analysis were extracted following extensive cardiac
498 perfusion with 10 mL of sterile PBS after cutting the right atrium. For flow cytometry and
499 MACs, leukocytes were isolated from whole brains after digestion in 0.05% collagenase
500 A (Sigma-Aldrich) and 10 mg/ml DNase I (Sigma- Aldrich), then purified via centrifugation
501 in 37% isotonic Percoll (Sigma-Aldrich) as described (PMID: 22729249). For MACs cells
502 were incubated with anti-F4/80 microbeads (Miltenyi) and separated with LS columns
503 (Miltenyi) per manufacturer's recommendations. FACs was performed on an LSRII
504 (Becton Dickinson) with analysis completed on FlowJo (Becton Dickinson).

505

506 **Immunofluorescence and FACs antibodies**

507

508 Brain tissue was fixed for 48 h in 4% PFA, followed by cryoprotection in 30% sucrose for
509 48 h. Brains were then frozen in optimal cutting temperature compound (Tissue-Tek) on
510 the freezing element of a Leica CM3050 S cryostat. 40-µm sections were sliced into 24-
511 well plates containing PBS with 0.05% sodium azide as previously described (PMID:
512 29941548). Slices were permeabilized and blocked with 0.25% Triton X-100 and 5%
513 Normal Donkey Serum (Sigma) for 1 hour followed by overnight incubation in 0.5% BSA
514 with primary antibody at 4° C. The following antibodies were used for
515 immunofluorescence staining: rabbit anti-Iba1 (1:300; CP-290; Biocare Medical), Goat
516 anti-Iba1(1:300; Abcam; ab5076), rat anti-CD68 (1:300; FA-11; Biolegend), Goat anti-IL-
517 33 (AF3626; R&D), Rabbit anti-Olig2 (1:500; AB 9610; Millipore Sigma), Rat-anti GFAP
518 (1:2000; 2.2B10; Thermo Fischer Scientific), Rabbit anti-Sox9 (1:500; AB5535; EMD
519 Millipore), Rabbit anti-NeuN (1:2000; D3S3I; Cell Signaling), Chicken anti-NeuN (1:300;
520 266 006; Synaptic Systems), Rabbit anti-C1q (1:300; ab182451; Abcam), Rabbit anti-
521 Cleaved caspase three (1:500; ab9661; Cell-Signaling), Rabbit anti-Phospho-c-Jun
522 (1:1000; D47G9; Cell Signaling), and Donkey anti-Mouse IgG (1:2000; A21203; Life
523 Technologies) . Slices were washed three times for 5 min, incubated for 2 h at room
524 temperature with the appropriate secondary antibodies (all Donkey-derived from Thermo
525 Fisher or Jackson Immunology using Alexaflours 488, 594, and 647; Life Technologies;
526 1:1,000), washed in PBS with DAPI (1:20,000; 62248; Thermo Fischer Scientific) washed
527 again three times for 5 min and mounted with Aquamount (14-390-5; Thermo Fischer
528 Scientific). Blinded image analysis including cell counting and MFI calculations were all
529 performed with ImageJ (National Institutes of Health).
530

531 Antibody cocktails for FACs staining were used at 1:100 in 2 mM EDTA (15-575-020;
532 Fischer Scientific) and 0.5% BSA (A7906-100G) or FOXP3/ Transcription Factor buffers
533 (00-5523-00; eBioscience) when staining for FOXP3. Antibodies used included GLAST
534 (130-123-555; Miltenyi), biotinylated ST2 (101001B; MD Bioscience), Streptavidin R-
535 Phycoerythrin (S21338; Thermo Scientific) and PE-conjugated NS4b tetramers (Fred
536 Hutch antibody core). Antibodies against CD3 (17A2; Fischer Scientific), CD4 (RM-4;
537 Fischer Scientific), CD8 (53-6.7; Fischer Scientific), CD44 (IM7; Fischer Scientific), CD69
538 (H1.2F3; Fischer Scientific), FOXP3 (FJK-16s; Fischer Scientific), F4/80 (T45-2342;
539 Fischer Scientific), NK1.1 (PK136; BioLegend), CD19 (1d3; Thermo Fisher), Ly6C (AL-
540 21; Fischer Scientific), Ly6G (1A8; Fischer Scientific), GITR (DTA-1; Fischer Scientific),
541 and CD25 (PC61; Fischer Scientific).
542
543 **Statistical analyses**
544
545 Statistical analyses comparing two groups at one time point were done using a student's
546 t-test in Prism software, v. 7.0a. One-way and two-way ANOVA were used appropriately
547 and were indicated. The number of mice per group, test used, and p values are denoted
548 in each Fig legend. Data was graphed using Prism software, v9 (GraphPad).
549
550 **Macrophage preparation and RNAsequencing**
551
552 After MACs isolation, brain macrophages were washed in PBS and cell pellets prepared
553 using the RNAqueous Micro kit (Ambion) per manufacturer's instruction. Total RNA was

554 concentrated by evaporation using an Eppendorf Vacufuge system and was then added
555 to lysis buffer from the SMART-Seq v4 Ultra Low Input RNA Kit for Sequencing (Takara).
556 Reverse transcription was performed followed by 20 cycles of PCR amplification to
557 generate full length amplified cDNA. Sequencing libraries were constructed using the
558 NexteraXT DNA sample preparation kit with unique dual indexes (Illumina) to generate
559 Illumina-compatible barcoded libraries. Libraries were pooled and quantified using a
560 Qubit® Fluorometer (Life Technologies). Sequencing of pooled libraries was carried out
561 on a NextSeq 2000 sequencer (Illumina) with paired-end 59-base reads, using a NextSeq
562 P3 sequencing kit (Illumina) with a target depth of 5 million reads per sample. Base calls
563 were processed to FASTQs on BaseSpace (Illumina), and a base call quality-trimming
564 step was applied to remove low-confidence base calls from the ends of reads. The
565 FASTQs were aligned to the GRCm38 mouse reference genome, using the STAR aligner,
566 and gene counts were generated using htseq-count. QC and metrics analysis was
567 performed using the Picard family of tools (v1.134).

568 Following generation of the counts matrix analyses were performed using R
569 (v4.2.2). The flow of analyses began with PCA analysis and visualization using the
570 PCAtools package (v2.10). Normalization and differential gene expression testing
571 analyses were performed using the DESeq2 package (v1.38.3) using the Wald statistical
572 testing method applied two condition comparisons. The DESeq2 results were then used
573 to generate ranks for gene set enrichment analysis (GSEA) using the fgsea package
574 (v1.24.0) to test for enrichment of gene ontology terms using the mouse ontology gene
575 sets (M5) collection downloaded from gsea-msigdb. The results from the GSEA and
576 differential gene expression testing were visualized using a combination of the ggplot2

577 (v3.4.0), pheatmap (v1.0.12), and EnhancedVolcano (v1.16.0) packages. All code
578 relevant to the data analyses in this study are available online at
579 https://github.com/OberstLab. The software used for the R analyses are publicly
580 available.
581
582
583 **Acknowledgments**
584 We thank Pooja Jain and Valerie Sheehan for technical assistance. We thank the lab of
585 Dr. Michael Gale, Jr., at the University of Washington for technical assistance and
586 discussion. We thank the viviarium staff of the University of Washington Department of
587 Comparative Medicine SLU 3.1 for their help and support. We thank all members of the
588 Oberst Lab for their input and support. We thank the Von Moltke and Pepper labs of the
589 University of Washington and the Ziegler lab of Benaroya Research Institute for mouse
590 lines used in this study. This work was supported by NIH/NIAID grants R01 AI132595 and
591 R21 AI178512 to AO. JMA was supported by the Helen Hay Whitney Foundation.
592
593 **Author Contributions**
594 Conceptualization: GTN, JMA, AO; Methodology: GTN, JMA, AO; Analysis: GTN, AO
595 (all), JMA (RNAseq data analysis); Investigation: GTN (all), JMA (RNAseq experimental
596 workflow); Resources: AO, SFZ; Writing-Original draft: GTN, AO; Writing-review and
597 editing: All authors.
598
599 **Declarations of Interest**

600 The authors declare no competing interests.

601

602 **References**

603 1. Chakarov S, Ginhoux F, Ble C. Review Determinants of Resident Tissue
604 Macrophage Identity and Function. 2020:957-970.
605 doi:10.1016/j.immuni.2020.05.014
606 2. Wolf SA, Boddeke HWGM, Kettenmann H. Microglia in Physiology and Disease.
607 *Annu Rev Physiol*. 2017;79:619-643. doi:10.1146/annurev-physiol-022516-
608 034406
609 3. Prinz M, Masuda T, Wheeler MA, Quintana FJ. Microglia and Central Nervous
610 System-Associated Macrophages mdash from Origin to Disease Modulation.
611 *Annu Rev Immunol*. 2021;39:251-277. doi:10.1146/annurev-immunol-093019-
612 110159
613 4. Klein RS, Garber C, Funk KE, et al. Neuroinflammation During RNA Viral
614 Infections. *Annu Rev Immunol*. 2019;37(1):73-95. doi:10.1146/annurev-immunol-
615 042718-041417
616 5. Lu Y, Basatemur G, Scott IC, et al. Interleukin-33 Signaling Controls the
617 Development of Iron-Recycling Macrophages. *Immunity*. 2020;52(5):782-793.e5.
618 doi:10.1016/j.immuni.2020.03.006
619 6. Vainchtein ID, Chin G, Cho FS, et al. Astrocyte-derived interleukin-33 promotes
620 microglial synapse engulfment and neural circuit development. *Science*. 2018:1-8.
621 7. Nguyen PT, Dorman LC, Pan S, et al. Microglial Remodeling of the Extracellular
622 Matrix Promotes Synapse Plasticity. *Cell*. 2020;182(2):388-403.e15.

623 doi:10.1016/j.cell.2020.05.050

624 8. Gadani SP, Walsh JT, Smirnov I, Zheng J, Kipnis J. The Glia-Derived Alarmin IL-
625 33 Orchestrates the Immune Response and Promotes Recovery following CNS
626 Injury. *Neuron*. 2015;85(4):703-709. doi:10.1016/j.neuron.2015.01.013

627 9. Still KM, Batista SJ, O'Brien CA, et al. Astrocytes promote a protective immune
628 response to brain Toxoplasma gondii infection via IL-33-ST2 signaling. *PLoS*
629 *Pathog*. 2020;16(10):1-28. doi:10.1371/journal.ppat.1009027

630 10. Garber C, Vasek MJ, Vollmer LL, Sun T, Jiang X, Klein RS. Astrocytes decrease
631 adult neurogenesis during virus-induced memory dysfunction via IL-1 article. *Nat*
632 *Immunol*. 2018;19(2):151-161. doi:10.1038/s41590-017-0021-y

633 11. Collins MH, Metz SW. Progress and Works in Progress: Update on Flavivirus
634 Vaccine Development. *Clin Ther*. 2017;39(8):1519-1536.
635 doi:10.1016/j.clinthera.2017.07.001

636 12. Petersen LR, Brault AC, Nasci RS. West Nile virus: Review of the literature.
637 *JAMA - J Am Med Assoc*. 2013;310(3):308-315. doi:10.1001/jama.2013.8042

638 13. Gould E, Solomon T. Pathogenic flaviviruses. *Lancet*. 2008;371(9611):500-509.
639 doi:10.1016/S0140-6736(08)60238-X

640 14. Vasek MJ, Garber C, Dorsey D, et al. A complement–microglial axis drives
641 synapse loss during virus-induced memory impairment. *Nature*.
642 2016;534(7608):538-543. doi:10.1038/nature18283

643 15. Garber C, Soung A, Vollmer LL, et al. T cells promote microglia-mediated
644 synaptic elimination and cognitive dysfunction during recovery from
645 neuropathogenic flaviviruses. *Nat Neurosci*. 2019. doi:10.1038/s41593-019-0427-

646 y
647 16. Funk KE, Klein RS. CSF1R antagonism limits local restimulation of antiviral CD8
648 + T cells during viral encephalitis. 2019;4:1-19.
649 17. Klein RS, Garber C, Howard N. Infectious immunity in the central nervous system
650 and brain function. *Nat Immunol*. 2017;18(2):132-141. doi:10.1038/ni.3656
651 18. Wang Y, Szretter KJ, Vermi W, et al. IL-34 is a tissue-restricted ligand of CSF1R
652 required for the development of Langerhans cells and microglia. *Nat Immunol*.
653 2012;13(8):753-760. doi:10.1038/ni.2360
654 19. Szretter KJ, Daniels BP, Cho H, et al. 2′-O methylation of the viral mRNA cap by
655 West Nile virus evades Ifit1-dependent and -independent mechanisms of host
656 restriction in vivo. *PLoS Pathog*. 2012;8(5). doi:10.1371/journal.ppat.1002698
657 20. Jordan I, Briese T, Fischer N, Lau JY, Lipkin WI. Ribavirin Inhibits West Nile Virus
658 Replication and Cytopathic Effect in Neural Cells. *J Infect Dis*. 2000;182(4):1214-
659 1217. doi:10.1086/315847
660 21. Schultz V, Cumberworth SL, Gu Q, et al. Zika virus infection leads to
661 demyelination and axonal injury in mature cns cultures. *Viruses*. 2021;13(1).
662 doi:10.3390/v13010091
663 22. Schultz V, Barrie JA, Donald CL, et al. Oligodendrocytes are susceptible to Zika
664 virus infection in a mouse model of perinatal exposure: Implications for CNS
665 complications. *Glia*. 2021;69(8):2023-2036. doi:10.1002/glia.24010
666 23. Bonilla W V, Fröhlich A, Senn K, et al. The Alarmin Interleukin-33 Drives
667 Protective Antiviral CD8+ TCell Responses. *Science (80-)*. 2012;(February).
668 doi:10.1126/science.1215418

669 24. Baumann C, Bonilla W V., Fröhlich A, et al. T-bet– and STAT4–dependent IL-33
670 receptor expression directly promotes antiviral Th1 cell responses. *Proc Natl Acad*
671 *Sci*. 2015;112(13):4056-4061. doi:10.1073/pnas.1418549112
672 25. Popovic B, Golemac M, Podlech J, et al. IL-33/ST2 pathway drives regulatory T
673 cell dependent suppression of liver damage upon cytomegalovirus infection. *PLoS*
674 *Pathog*. 2017;13(4):1-23. doi:10.1371/journal.ppat.1006345
675 26. Slon Campos JL, Mongkolsapaya J, Screaton GR. The immune response against
676 flaviviruses. *Nat Immunol*. 2018. doi:10.1038/s41590-018-0210-3
677 27. Lanteri MC, O'Brien KM, Purtha WE, et al. Tregs control the development of
678 symptomatic West Nile virus infection in humans and mice. *J Clin Invest*.
679 2009;119(11):3266-3277. doi:10.1172/JCI39387
680 28. Shrestha B, Diamond M. Role of CD8+ T cells in control of West Nile virus
681 infection. *J Virol*. 2004;78(15):8312-8321. doi:10.1128/JVI.78.15.8312
682 29. Gadani SP, Smirnov I, Smith AT, Overall CC, Kipnis J. Characterization of
683 meningeal type 2 innate lymphocytes and their response to CNS injury. *J Exp*
684 *Med*. 2016:1-14.
685 30. Webster KE, Walters S, Kohler RE, et al. In vivo expansion of T reg cells with IL-
686 2-mAb complexes: induction of resistance to EAE and long-term acceptance of
687 islet allografts without immunosuppression. *J Exp Med*. 2009;206(4):751-760.
688 doi:10.1084/jem.20082824
689 31. He D, Xu H, Zhang H, Rozenblatt-Rosen O, Regev A, Kuchroo VK. Disruption of
690 the IL-33-ST2-AKT signaling axis impairs neurodevelopment by inhibiting
691 microglial metabolic adaptation and phagocytic function. *Immunity*. 2022:1-15.

692 doi:10.1016/j.immuni.2021.12.001

693 32. Stephan AH, Barres B a., Stevens B. The Complement System: An Unexpected
694 Role in Synaptic Pruning During Development and Disease. *Annu Rev Neurosci*.
695 2012;35(1):369-389. doi:10.1146/annurev-neuro-061010-113810

696 33. Goldmann T, Wieghofer P, Müller PF, et al. A new type of microglia gene
697 targeting shows TAK1 to be pivotal in CNS autoimmune inflammation. *Nat*
698 *Neurosci*. 2013;16(11):1618-1626. doi:10.1038/nn.3531

699 34. Norris GT, Smirnov I, Filiano AJ, et al. Neuronal integrity and complement control
700 synaptic material clearance by microglia after CNS injury. 2018;215(7).
701 doi:10.1084/jem.20172244

702 35. Liu B, Tai Y, Achanta S, et al. IL-33/ST2 signaling excites sensory neurons and
703 mediates itch response in a mouse model of poison ivy contact allergy. *Proc Natl*
704 *Acad Sci*. 2016;113(47):E7572-E7579. doi:10.1073/pnas.1606608113

705 36. Getts MT, Müller M, Rana S, et al. Ly6c + “inflammatory monocytes” are
706 microglial precursors recruited in a pathogenic manner in West Nile virus
707 encephalitis . *J Exp Med*. 2008;205(10):2319-2337. doi:10.1084/jem.20080421

708 37. Terry RL, Getts DR, Deffrasnes C, van Vreden C, Campbell IL, King NJC.
709 Inflammatory monocytes and the pathogenesis of viral encephalitis. *J*
710 *Neuroinflammation*. 2012;9:1-10. doi:10.1186/1742-2094-9-270

711 38. Getts DR, Terry RL, Getts MT, et al. Targeted blockade in lethal West Nile virus
712 encephalitis indicates a crucial role for very late antigen (VLA)-4-dependent
713 recruitment of nitric oxide-producing macrophages. *J Neuroinflammation*.
714 2012;9:2-9. doi:10.1186/1742-2094-9-246

715 39. Yarza R, Vela S, Solas M, Ramirez MJ. c-Jun N-terminal kinase (JNK) signaling
716 as a therapeutic target for Alzheimer's disease. *Front Pharmacol*. 2016;6(JAN):1-
717 12. doi:10.3389/fphar.2015.00321
718 40. Manning AM, Davis RJ. Targeting JNK for therapeutic benefit: From junk to gold?
719 *Nat Rev Drug Discov*. 2003;2(7):554-565. doi:10.1038/nrd1132
720 41. Zhang Y, Chen K, Sloan S a., et al. An RNA-Sequencing Transcriptome and
721 Splicing Database of Glia, Neurons, and Vascular Cells of the Cerebral Cortex. *J*
722 *Neurosci*. 2014;34(36):11929-11947. doi:10.1523/JNEUROSCI.1860-14.2014
723 42. Ofengeim D, Ito Y, Najafov A, et al. Activation of necroptosis in multiple sclerosis.
724 *Cell Rep*. 2015;10(11):1836-1849. doi:10.1016/j.celrep.2015.02.051
725 43. Lüthi AU, Cullen SP, McNeela EA, et al. Suppression of Interleukin-33 Bioactivity
726 through Proteolysis by Apoptotic Caspases. *Immunity*. 2009;31(1):84-98.
727 doi:10.1016/j.immuni.2009.05.007
728 44. Kearley J, Silver JS, Sanden C, et al. Cigarette smoke silences innate lymphoid
729 cell function and facilitates an exacerbated type I interleukin-33-dependent
730 response to infection. *Immunity*. 2015;42(3):566-579.
731 doi:10.1016/j.immuni.2015.02.011
732 45. Bellver-Landete V, Bretheau F, Mailhot B, et al. Microglia are an essential
733 component of the neuroprotective scar that forms after spinal cord injury. *Nat*
734 *Commun*. 2019;10(1). doi:10.1038/s41467-019-08446-0
735 46. Rasley A, Tranguch SL, Rati DM, Marriot I. Murine Glia Express the
736 Immunosuppressive Cytokine, Interleukin-10, Following Exposure to Borrelia
737 burgdorferi or Neisseria meningitidis. *Glia*. 2006;479(March):132. doi:10.1002/glia

738 47. Trang T, Beggs S, Salter MW. Brain-derived neurotrophic factor from microglia: A
739 molecular substrate for neuropathic pain. *Neuron Glia Biol*. 2012;7(1):99-108.
740 doi:10.1017/S1740925X12000087
741 48. Medzhitov R, Schneider DS, Soares MP. Disease Tolerance as a Defense
742 Strategy. *Science (80-)*. 2012;335(6071):165-184.
743 doi:10.1126/science.1214935.Disease
744 49. Ayres JS. The Biology of Physiological Health. *Cell*. 2020;181(2):250-269.
745 doi:10.1016/j.cell.2020.03.036
746
747 **Figure Legends**
748
749 **Fig 1. The IL-33 pathway promotes survival upon neuroinvasive flavivirus infection,**
750 **independent of viral control**
751 (A) Survival analysis in *Il33*$^{-/-}$, *Il1rl1*$^{-/-}$, and B6/J mice following intracranial infection with
752 2e4 PFU WNV-E218A.
753 (B) WNV Viral titers from indicated CNS components and tissues of mice 7 days post-
754 infection via plaque assay on BHK cells.
755 (C) Survival analysis in *Il33*$^{-/-}$, *Il1rl1*$^{-/-}$, and B6/J mice following intracranial infection of
756 1e6 PFU ZIKV-Dakar.
757 (D) ZIKV Viral titers from indicated CNS components and tissues of mice 7 days post-
758 infection via plaque assay on Vero cells.
759 (E) WNV Viral titers from indicated CNS components and tissues of mice 10 days post-
760 infection via plaque assay on BHK cells

761 Data are representative of 3 pooled independent experiments (error bars, SEM). * $p <$
762 0.05, ** $p < 0.01$, *** $p < 0.001$ (A, C) (Gehan-Breslow-Wilcoxon test) (B, D, E) (2-way
763 ANOVA with Holm-Sidak Multiple comparisons).
764
765 **Fig 2. Oligodendrocyte-derived IL-33 promotes survival to neurotropic flavivirus**
766 **infection**
767 (A) Ratios of IL-33+ cells in indicated brain regions in adult B6/J mice with HBSS injection.
768 (B) Representative immunofluorescent images of IL-33+ cell loss in B6/J Hippocampal
769 CA3 7 days post intracranial infection with WNV-E218A (20x magnification, scale bars,
770 100 microns). Arrowheads indicate IL-33+Olig2+ and arrows IL-33+GFAP+ cells.
771 (C) Quantification of IL-33 positivity in Olig2+ and GFAP+ in B6/J Hippocampal CA3 7
772 days post intracranial infection with WNV-E218A.
773 (D) Representative images of Olig2+ cell loss in indicated brain regions 7 days post
774 intracranial infection with WNV-E218A (20x magnification, scale bars, 100 microns).
775 (E) Quantification of Olig2+ cell number in Hippocampal CA3 7 days post intracranial
776 infection with WNV-E218A.
777 (F) Survival analysis of mice with oligodendrocyte-specific deletion of IL-33 following
778 intracranial infection of 2e4 PFU WNV-E218A.
779 (A-E) Data are representative of two independent experiments. (F) Data are
780 representative of 3 pooled independent experiments (error bars, SEM). * $p < 0.05$, ** $p <$
781 0.01, *** $p < 0.001$. (C and E) two-tailed student's T test (F) (Gehan-Breslow-Wilcoxon
782 test).
783

784 **Fig 3. IL-33/ST2 signaling on adaptive immune cells does not impact host survival**
785 **following intracranial flavivirus infection**
786 (A) Cell number and CD44/CD69 gMFI of indicated adaptive immune cell types per ½
787 brain by FACs 7 days post intracranial infection with WNV-E218A.
788 (B) Cell number and CD44/CD69 gMFI of indicated adaptive immune cell types per ½
789 brain by FACs 7 days post intracranial infection with ZIKV-Dakar.
790 (C) Percent ST2+ and ST2 gMFI of indicated immune cell types 7 days post vehicle
791 injection.
792 (D) Percent ST2+ and ST2 gMFI of immune cells 7 days post intracranial infection with
793 WNV-E218A.
794 (E) Survival analysis of mice with Treg deletion of ST2 following intracranial ZIKV-Dakar
795 infection.
796 Data are representative of 2 pooled independent experiments (error bars, SEM). * $p <$
797 0.05, ** $p < 0.01$, *** $p < 0.001$ (A, B) (2-way ANOVA with Holm-Sidak Multiple
798 comparisons) (C, D) (One-way ANOVA with Holm-Sidak Multiple comparisons). (E)
799 (Gehan-Breslow-Wilcoxon test)
800
801
802
803 **Fig 4. IL-33/ST2 signaling is necessary for microglial activation and host defense**
804 **following CNS flavivirus infection.**

805 (A) Representative immunofluorescent images of microglial activation and IL-33 cell loss
806 in hippocampal CA3 with increasing doses of intracranial WNV-E218A (20x magnification,
807 scale bars, 100 microns).
808 (B) Quantification of IL-33+ cell number, macrophage activation, and their correlation in
809 hippocampal CA3 with increasing doses of intracranial WNV-E218A.
810 (C) Representative immunofluorescent images of Iba1+ microglia in B6/J and *Il1rl1*$^{-/-}$
811 mice 7 days post-infection with WNV-E218A (20x magnification, scale bars, 100 microns).
812 (D) Quantification of Iba1 by MFI in indicated brain regions of B6/J and *Il1rl1*$^{-/-}$ mice 7
813 days post-infection with WNV-E218A.
814 (E) Survival analysis of mice with microglial-specific deletion of ST2 following intracranial
815 infection with WNV-E218A.
816 Data are representative of 2 and 3 (E) pooled independent experiments (error bars, SEM).
817 * $p < 0.05$, ** $p < 0.01$, *** $p < 0.001$. (B, D) (2-way ANOVA with Holm-Sidak Multiple
818 comparisons and Pearson's Correlation) (E) (Gehan-Breslow-Wilcoxon test).
819
820 **Fig 5. *Il33*$^{-/-}$ hippocampal macrophages exhibit enhanced inflammatory and cell**
821 **stress responses acutely during CNS WNV infection.**
822 (A) Scheme of hippocampal macrophage isolation and RNAsequencing following
823 intracranial WNV-E218A infection of B6/J and *Il33*$^{-/-}$ mice.
824 (B) Principal Component Analysis of RNAseq samples.
825 (C) Volcano plot showing differential gene expression in *Il33*$^{-/-}$ vs. B6/J hippocampal
826 macrophages post-infection.

827 (D) Top 20 Hallmark gene sets enriched in *Il33*$^{-/-}$ relative to B6/J hippocampal
828 macrophages post-infection.
829
830 **Fig 6. Disruption of IL-33 signaling during CNS WNV infection induces brain**
831 **macrophage apoptosis and neuronal pathology.**
832 (A) %ZombieNIR+ dying cell populations of indicated type by FACs analysis of brain
833 homogenates 7 days post-infection with WNV-E218A in B6/J and *Il1rl1*$^{-/-}$ mice.
834 (B) Representative images of CC3+ CA3 hippocampal brain macrophages 7 days post-
835 infection with WNV-E218A in B6/J and *Il33*$^{-/-}$ mice (20x magnification, scale bars, 100
836 microns). Arrowheads indicate Iba1-CC3+ while arrows indicate Iba1+CC3+ cells.
837 (C) Quantification of CC3+ CA3 hippocampal brain macrophages.
838 (D) Quantification of monocyte count by FACs analysis of brain homogenates in B6/J
839 and *Il1rl1*$^{-/-}$ mice 7 days post WNV-E218A infection.
840 (E) Representative images of monocyte engraftment in hippocampal CA3 and
841 cerebellum of B6/J and *Il1rl1*$^{-/-}$ mice 7 days post WNV-E218A infection (20x
842 magnification, scale bars, 100 microns). Arrowheads indicate Iba1-CD68+ cells.
843 (F) Quantification of CD68+Iba1- monocytes in hippocampal CA3 and cerebellum.
844 (G) Representative images of pCJun+ cells and IgG deposition in hippocampal CA3 7
845 days post-infection with WNV-E218A in B6/J and *Il33*$^{-/-}$ mice (20x magnification, scale
846 bars, 100 microns). Arrowheads indicated pCJun+ cells.
847 (H) Quantification of pCJun+ cells and IgG MFI.

848 (I) Representative images of pCJun+ projections and GFAP+ cells hippocampal CA3 7
849 days post-infection with WNV-E218A in B6/J and *Il33*$^{-/-}$ mice (20x magnification, scale
850 bars, 100 microns).
851 (J) Quantification of GFAP+ area and pCJun+ projection area.
852 (K) Representative images of CC3+ neurons in hippocampal CA3 and cerebellum of
853 B6/J and *Il1rl1*$^{-/-}$ mice 7 days post WNV-E218A infection (20x magnification, scale bars,
854 100 microns). Arrowheads indicate NeuN+CC3+ cells.
855 (L) Quantification of CC3+ neuron number in CA3 and cerebellum.
856 Data are representative of 2 (A-F) independent and 2 (G-N) pooled independent
857 experiments (error bars, SEM). * $p < 0.05$, ** $p < 0.01$, *** $p < 0.001$. (A, C, H)
858 (two-tailed T test) (E, G, J, L) (Two-way ANOVA with Holm-Sidak multiple
859 comparisons).
860
861 **Supplemental Figures**
862 **Fig S1 (related to Fig 1). The IL-33 pathway improves disease outcomes across**
863 **multiple models of flavivirus infection**
864 (A) Survival analysis of adult B6/J mice exposed to increasing doses of intracranial WNV-
865 E218A and WNV-Tx.
866 (B) Weight loss of *Il33*$^{-/-}$, *Il1rl1*$^{-/-}$, and B6/J mice following 2e4 PFU WNV-E218A
867 intracranial infection.
868 (C) Weight loss of *Il33*$^{-/-}$, *Il1rl1*$^{-/-}$, and B6/J mice following 1e6 PFU ZIKV-Dakar
869 intracranial infection.

870 (D) Survival analysis of *Il1rl1*$^{-/-}$ and B6/J mice following footpad infection with 100 PFU
871 WNV-Tx.
872 (E) Weight loss of *Il1rl1*$^{-/-}$ and B6/J mice following footpad infection with 100 PFU WNV-
873 Tx.
874 Data are representative of 3 pooled independent experiments (error bars, SEM). * $p <$
875 0.05, ** $p < 0.01$, *** $p < 0.001$ (A, D) (Gehan-Breslow-Wilcoxon test) (B, C, E) (2-way
876 ANOVA with Holm-Sidak Multiple comparisons).
877
878 **Fig S2 (related to Fig 2). Deletion of IL-33 in oligodendrocytes with tamoxifen**
879 **treatment of *Plp1*$^{ERT2Cre/+}$::*Il33*$^{fl/fl}$ mice**
880 (A) GFAP+ cell number by immunohistochemistry following intracranial infection with
881 increasing doses of WNV-E218A.
882 (B) Scheme for tamoxifen injections to induce IL-33 excision and representative images
883 of IL-33 loss in cortical oligodendrocytes following tamoxifen treatment (20x
884 magnification, scale bars, 50 microns). Arrowheads Indicate Olig2+IL-33+ cells.
885 (C) Quantification of total cortical oligodendrocyte number and IL-33+ oligodendrocytes
886 following tamoxifen injection.
887 Data are representative of 3 pooled independent experiments (error bars, SEM). *** $p <$
888 0.001. (C) two-tailed student's T test.
889
890 **Fig S3 (related to Fig 3). ST2 is highly expressed on adaptive immune subsets, but**
891 **this expression is dispensible for host survival.**
892 (A) Scheme for CD8 T cell depletion during intracranial WNV-E218A infection.

893 (B) Peripheral blood counts 6 DPI to confirm CD8 depletion.

894 (C) Survival analysis of mice with CD8 T cell depletion and WNV-E218A intracranial
895 infection.

896 (D) Weight change in mice with CD8 T cell depletion and control IgG injection following
897 WNV-E218A intracranial infection.

898 (E) Representative FACs plots and gating strategy for indicated cell types from brain
899 homogenate 7 days post intracranial WNV-E218A infection.

900 (F) Representative FACs plots of ST2 expression on indicated cell types from B6/J and
901 *Il1rl1*$^{-/-}$ brain homogenate 7 days post intracranial WNV-E218A infection.

902 (G) Quantification of ST2 excision on splenic and liver Tregs of indicated genotype one-
903 month post tamoxifen treatment.

904 (H) Weight change in mice with Treg ST2 deletion following intracranial infection with
905 ZIKV-Dakar

906 (I) Scheme and cell number from peripheral blood of indicated immune cells following IL-2
907 complex treatment and WNV-E218A infection at 9 DPI.

908 (J) gMFI of CD25 and GITR on peripheral blood Tregs at 9 DPI with WNV-E218A and
909 IL-2 complex treatment.

910 (K) Survival analysis of mice with control or IL-2 complex treatment following intracranial
911 infection with WNV-E218A.

912 (L) Weight change in mice with control or IL-2 complex treatment after intracranial
913 infection with WNV-E218A.

914 Data are representative of 2 pooled independent experiments (error bars, SEM). * $p < 0.05$, ** $p < 0.01$, *** $p < 0.001$. (B, D, G, J, H, L) (2-way ANOVA with Holm-Sidak Multiple
915 comparisons) (C, K) (Gehan-Breslow-Wilcoxon test) (I) (Student's two-tailed t Test).
916
917 **Fig S4 (related to Fig 4). Phenotypes of ST2 signaling on microglial activation**
918 **during CNS Flavivirus infection.**
919
920 (A) Representative immunofluorescent images of Iba1+ brain macrophages in B6/J and
921 *Il1rl1*$^{-/-}$ mice 7 days post vehicle injection (20x magnification, scale bars, 100 microns).
922 (B) Quantification of Iba1 gMFI in vehicle injected mice of indicated brain regions.
923 (C) Representative immunofluorescent images of Iba1+ brain macrophages in B6/J and
924 *Il1rl1*$^{-/-}$ mice 10 days post WNV-E218A infection (20x magnification, scale bars, 100
925 microns).
926 (D) Quantification of Iba1 MFI 10 days post WNV-E218A infection in hippocampal CA3 of
927 B6/J and *Il1rl1*$^{-/-}$ mice.
928 (E) Representative immunofluorescent images of C1q deposition in hippocampal CA3 of
929 B6/J and *Il33*$^{-/-}$ mice 7 days post-infection (20x magnification, scale bars, 100 microns).
930 (F) Quantification of C1q gMFI by immunofluorescence in hippocampal CA3 of B6/J and
931 *Il33*$^{-/-}$ mice 7 days post-infection.
932 (G) Representative FACs plots of microglia from CX3CR1$^{ERT2Cre/+::}$ *Il1rl1*$^{fl/fl}$ 30 days post
933 tamoxifen treatment and following CD11b enrichment by MACs.
934 (H) Quantification of MACs enrichment efficiency.
935 (I) Quantification of *Il1rl1* signal by qRT-PCR of sorted microglia 30 days post tamoxifen
936 treatment and following CD11b enrichment by MACs.

937 (J) Weight change in CX3CR1$^{ERT2Cre/+::}$ *Il1rl1*$^{fl/fl}$ mice following intracranial infection of
938 WNV-E218A.
939 (K) Survival analysis of mice with neuronal *Il1rl1* deletion following intracranial infection
940 with WNV-E218A.
941 (L) Weight change of mice with neuronal *Il1rl1* deletion following intracranial infection with
942 WNV-E218A.
943 Data are representative of 2 (A-F) independent and 2 (G-N) pooled independent
944 experiments (error bars, SEM). * $p < 0.05$, ** $p < 0.01$, *** $p < 0.001$. (B, F, H, L) (two-
945 tailed T test) (D, I, J, N) (Two-way ANOVA with Holm-Sidak multiple comparisons) (M)
946 (Gehan-Breslow-Wilcoxon test).
947
948 **Fig S5 (related to Fig 5). Hallmark pathways enriched in *Il33*$^{-/-}$ hippocampal**
949 **macrophages during WNV infection.**
950 (A) Volcano plot showing enriched genes in *Il33*$^{-/-}$ hippocampal macrophages relative to
951 B6/J with vehicle injection.
952 (B) Top 20 significantly enriched Hallmark gene sets by GSEA of *Il33*$^{-/-}$ and B6/J
953 hippocampal macrophages post-infection in vehicle-injected samples.
954 (C) Heatmap of Inflammatory Response pathway genes in indicated samples.
955 (D) Heatmap of Fatty Acid Metabolism pathway genes in indicated samples.
956 (E) Heatmap of Oxidative Phosphorylation pathway genes in indicated samples.
957 (F) Heatmap of Hypoxia pathway genes in indicated samples.
958 (G) Heatmap of Apoptosis pathway genes in indicated samples.
959

960 **Fig S6 (related to Fig 6) IL-33 signaling prevents brain macrophage apoptosis**

961 **following intracranial ZIKV-Dakar infection.**

962 (A) Representative images of CC3+ hippocampal CA1 brain macrophages in B6/J and

963 *Il33*$^{-/-}$ mice 7 days post-infection with WNV-E218A (20x magnification, scale bars, 100

964 microns).

965 (B) Quantification of CC3+ hippocampal CA1 brain macrophages in B6/J and *Il33*$^{-/-}$ mice.

966
967

968

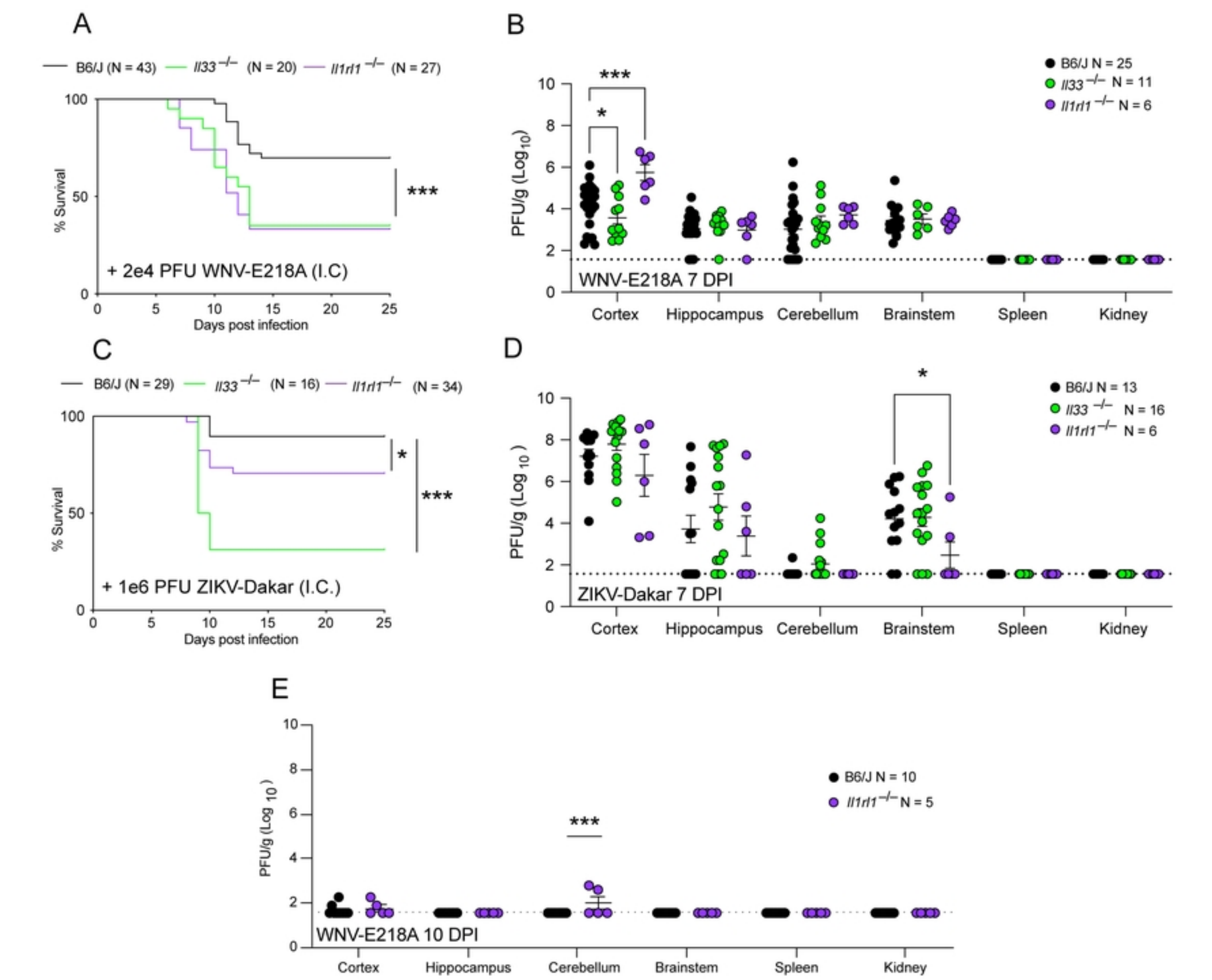

Figure 1. The IL-33 pathway promotes survival upon neuroinvasive flavivirus infection, independent of viral control

Figure 1

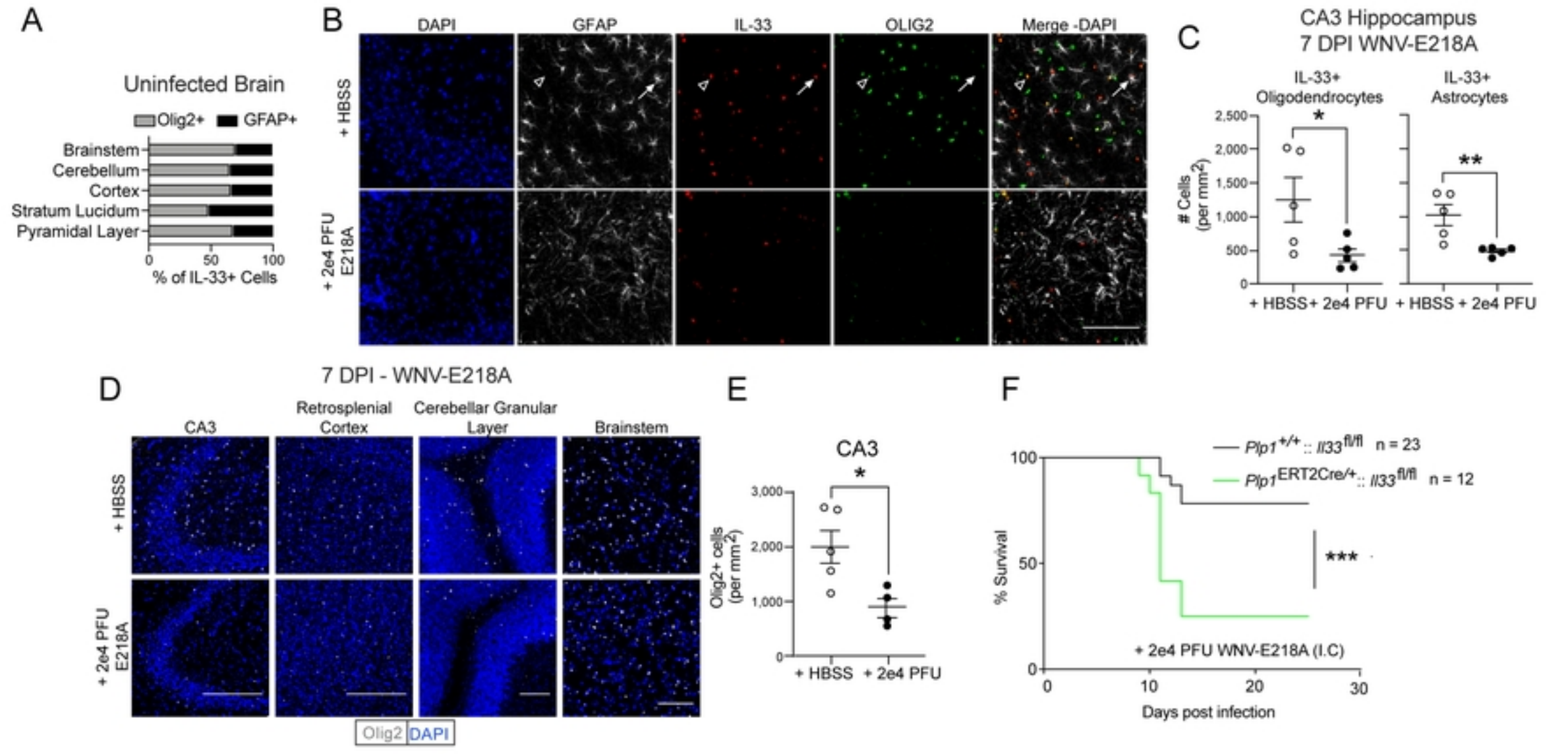

Figure 2. Oligodendrocyte-derived IL-33 promotes survival to neurotropic flavivirus infection

Figure 2

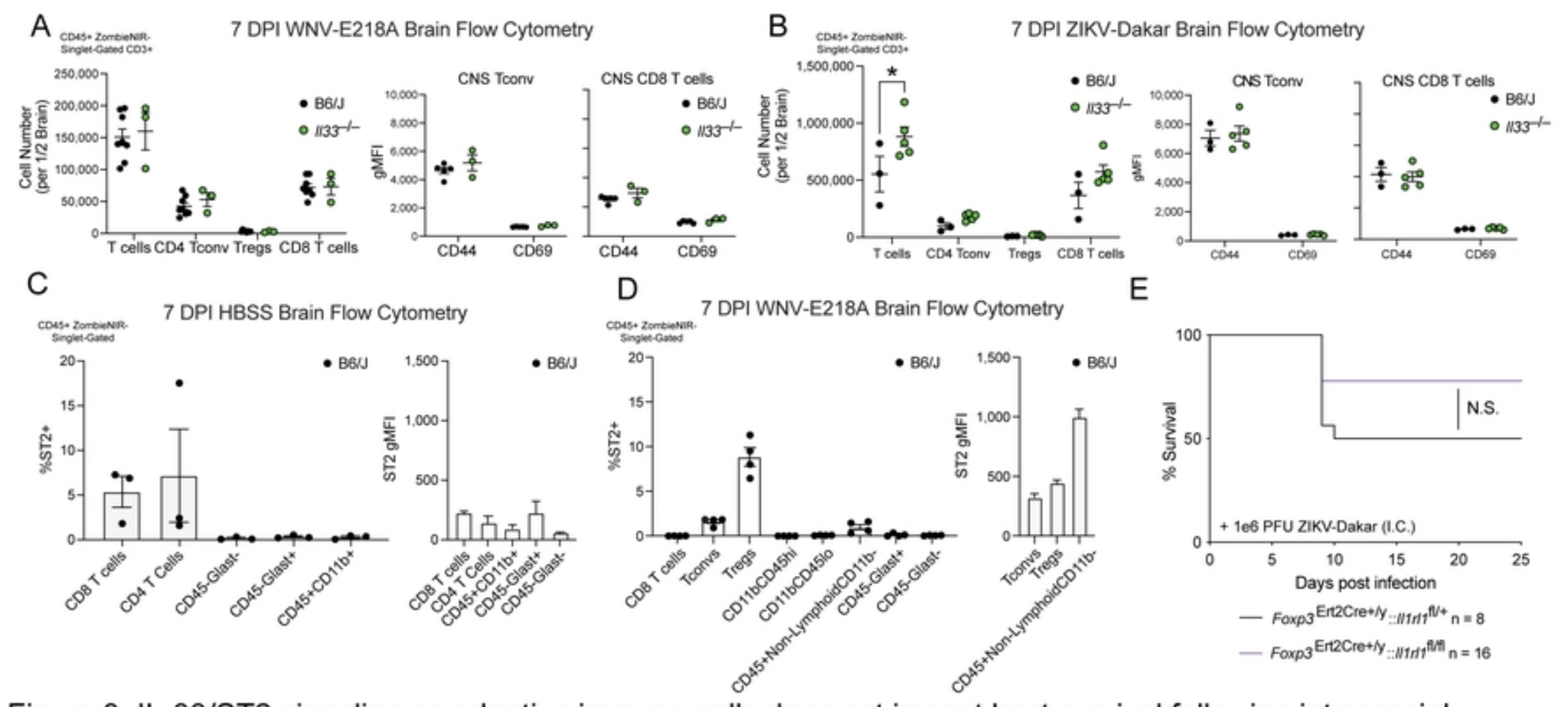

Figure 3. IL-33/ST2 signaling on adaptive immune cells does not impact host survival following intracranial flavivirus infection

Figure 3

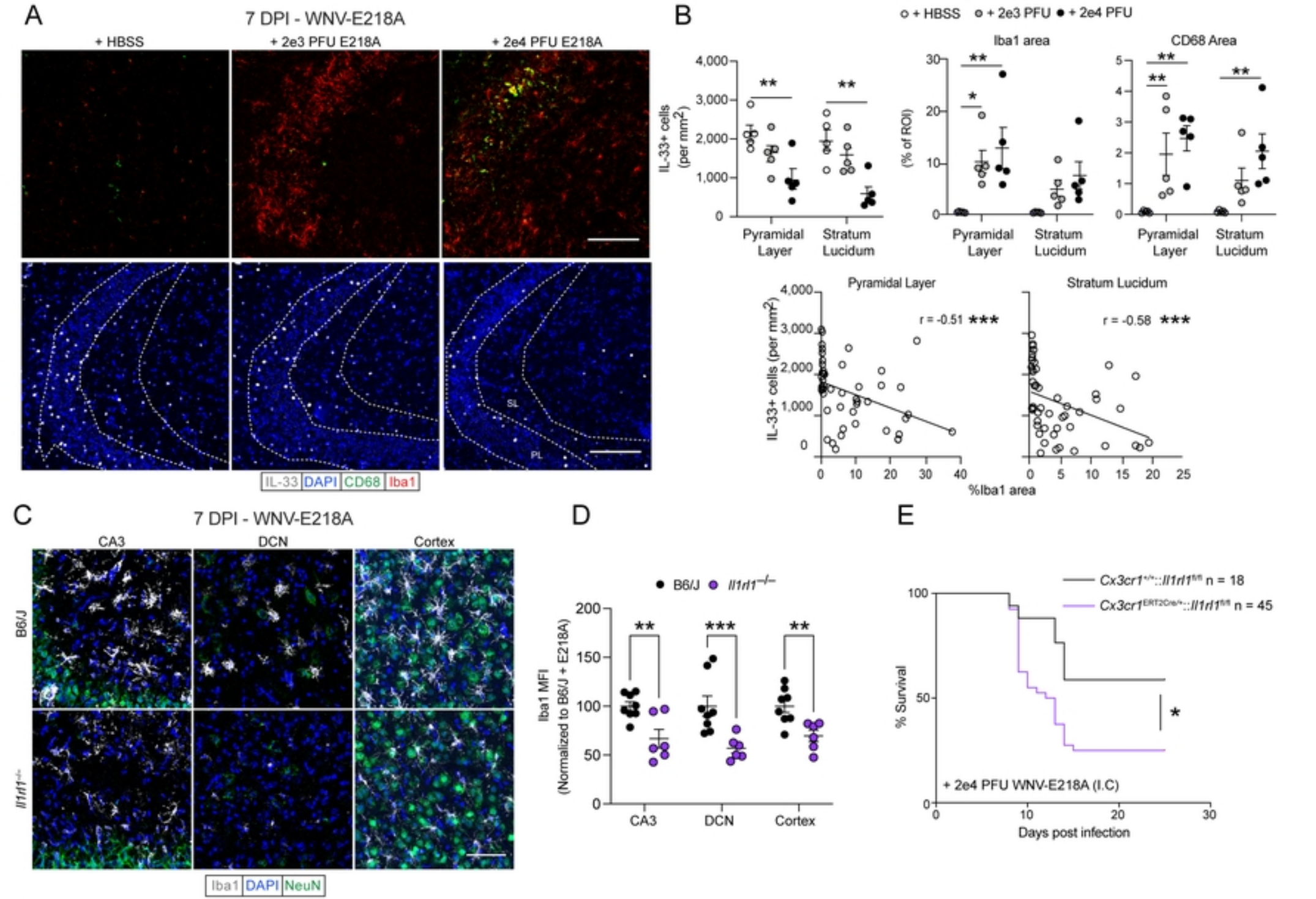

Figure 4. IL-33/ST2 signaling is necessary for microglial activation and host defense following CNS flavivirus infection.

Figure 4

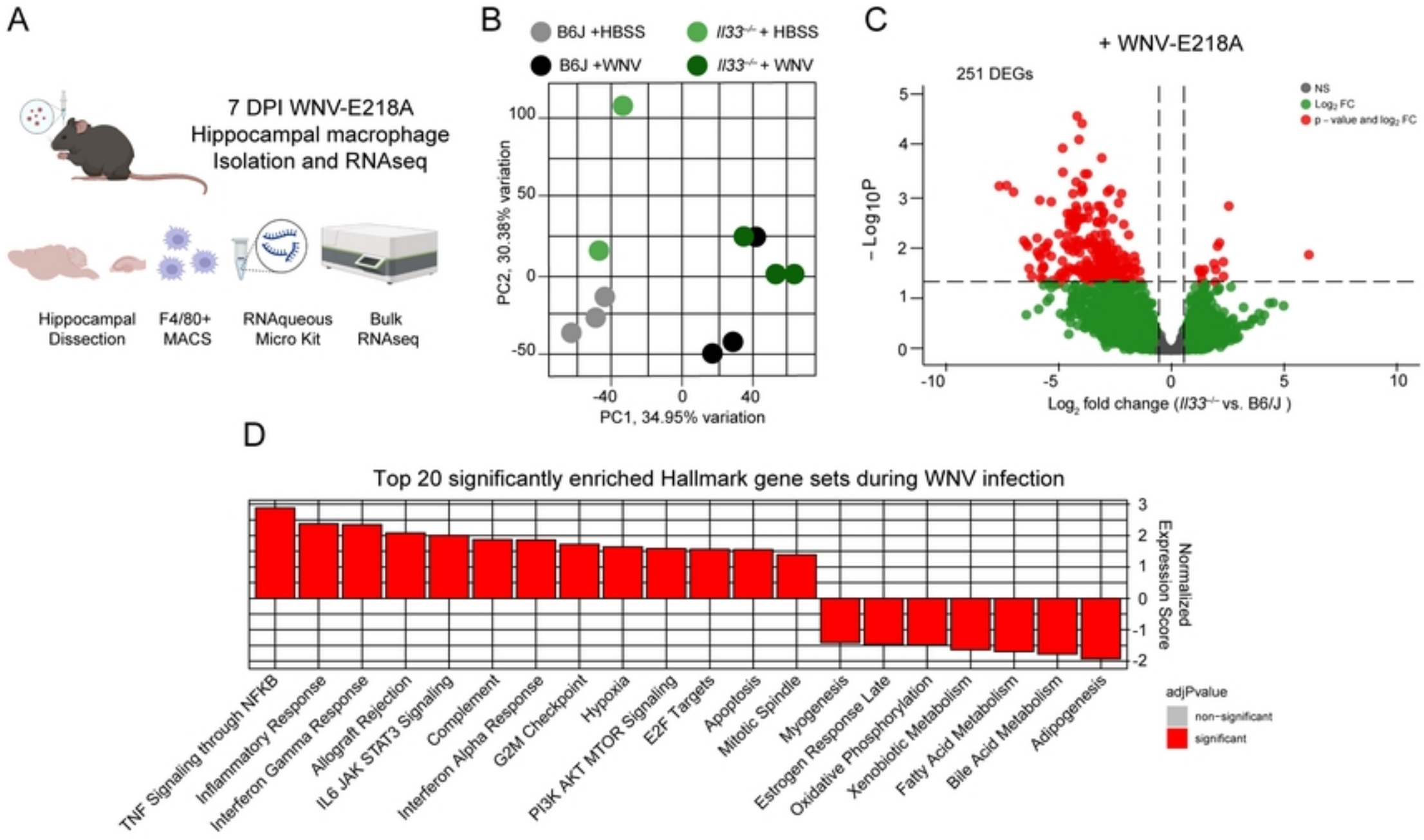

Figure 5. *Il33*$^{-/-}$ Hippocampal macrophages exhibit enhanced inflammatory and cell stress responses acutely during CNS WNV infection.

Figure 5

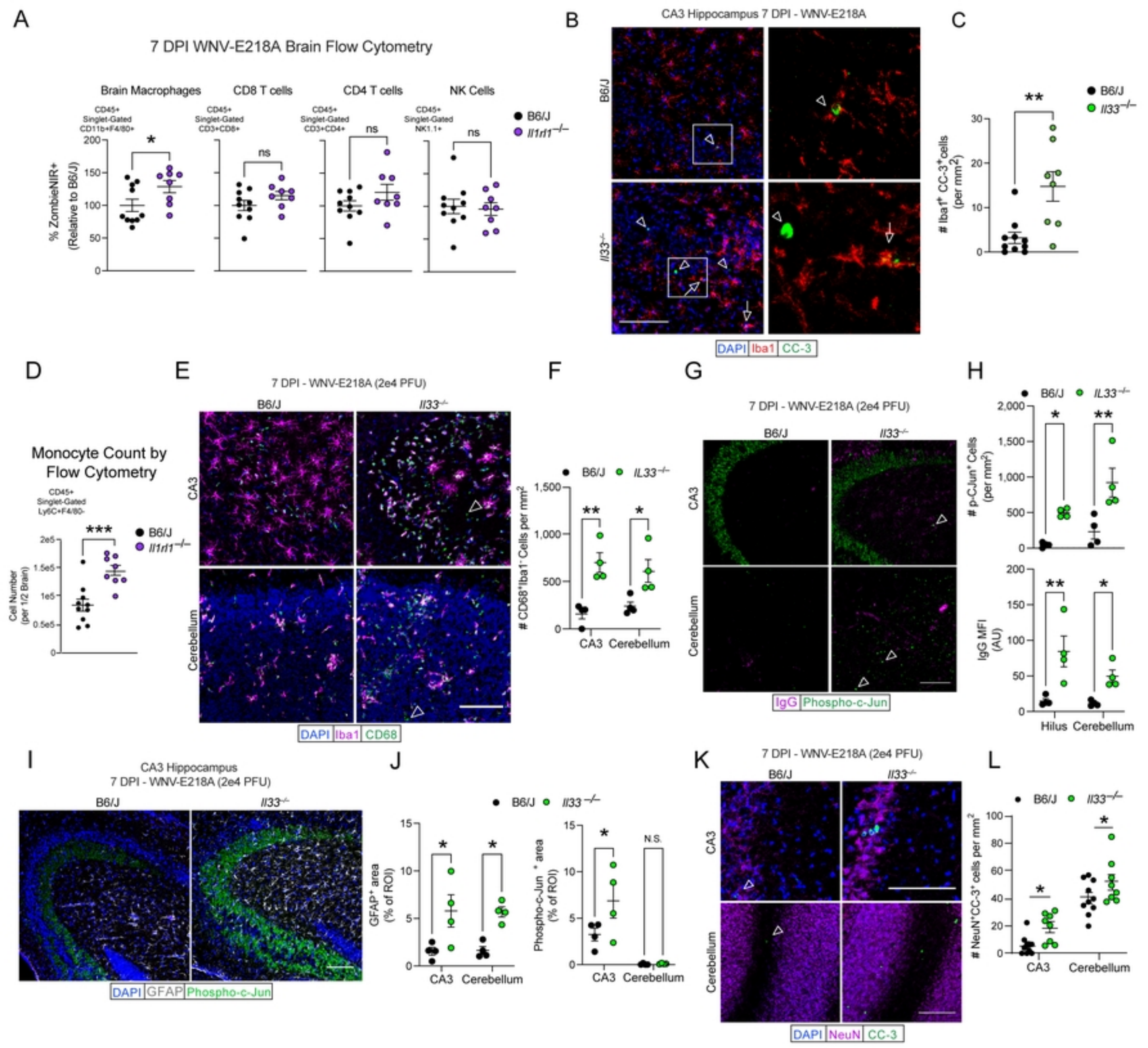

Figure 6. Disruption of IL-33 signaling during CNS WNV infection induces brain macrophage apoptosis and neuronal pathology.

Figure 6